Numerical study of flashing pipe flow using a TFM-PBM coupled method:Effect of interfacial heat transfer and bubble coalescence and breakup

Li, J.; Liao, Y.; Zhou, P.; Lucas, D.; Li, Q.;

Originally published:

June 2023

International Journal of Thermal Sciences 193(2023), 108504

DOI: https://doi.org/10.1016/j.ijthermalsci.2023.108504

Perma-Link to Publication Repository of HZDR:

https://www.hzdr.de/publications/Publ-37130

Numerical study of flashing pipe flow using a TFM-PBM coupled method: Effect of interfacial heat transfer and bubble coalescence and breakup

Jiadong Li[a, b], Yixiang Liao[b, *], Ping Zhou[a], Dirk Lucas[b], Qing Li[a, †]

[a] School of Energy Science and Engineering, Central South University, 410083 Changsha, China

[b] Helmholtz-Zentrum Dresden-Rossendorf, Institute of Fluid dynamics, Bautzner Landstraße 400, 01328 Dresden, Germany

ABSTRACT

In the present work, the two-fluid model (TFM) is coupled with the population balance model (PBM) to trace the spatial and temporal change of bubble size and interfacial area concentration (IAC) in flashing flows. The model is first validated for bubble growing in stagnant superheated liquid, and satisfactory predictions of the bubble size under low and moderate superheat are obtained. It is then applied to flashing pipe flows, which are characterized by low superheat and high turbulence intensities. The results show that in these cases, coalescence and breakup are important phenomena changing the bubble size distribution in addition to growth. The neglect of their contribution leads to a significant under-prediction of the bubble size and consequently over-prediction of IAC. In addition, choosing an appropriate closure for interfacial heat transfer coefficient (HTC) is another key point in flashing simulation. In high-Reynolds cases (e.g. $Re>10^6$), the enhancement due to turbulence is non-negligible.

Keywords

Flashing flow; Interfacial area concentration; Interfacial heat transfer; Two-fluid model; Population balance model

[*] Corresponding author.
E-mail address: y.liao@hzdr.de (Y. Liao).
[†] Corresponding author.
E-mail address: qingli@csu.edu.cn (Q. Li).

1. Introduction

Flashing (or flash boiling) is initiated by depressurization of an initially sub-cooled or saturated liquid. Flashing phenomena are commonly encountered in many industrial and manufacturing scenarios, such as geothermal energy recovery[1,2], seawater desalination[3,4], fuel atomization[5–7], and spray cooling[8,9]. On the other hand, flashing also occurs with the failure or accidents of high-temperature and high-pressure equipment. One example is the loss of coolant accident (LOCA) in the primary circuit of the pressurized water reactor (PWR). The fast phase change during LOCA process is of great significance for determining the leak rate of the reactor coolant, and affects the core safety within the PWR system[10]. Another example is the flashing instability induced water hammer (FIIWH) phenomenon, causing pressure and flow oscillations in the riser tube of the open natural circulation system[11]. Flow characteristics in the above flashing situations are strongly influenced by the interfacial interactions and exchanges. A better understanding of the mechanisms behind flashing flows not only benefits the industrial applications, but also ensure the safe operation of those systems.

Efforts have been made in the past to develop various methods to describe interfacial transfer behaviors during flashing processes. One of the most promising tools is the two-fluid model (TFM), which is formulated by considering the gas and liquid phases as interpenetrating continua and solving their transport equations separately. The interfacial transfer can be accounted for by additional constitutive relations also referred to as closures. Basically, the volumetric interfacial transfer rate is proportional to the interfacial area concentration (IAC), which is defined as the interfacial area per unit volume of the mixture. Therefore, the performance of TFM heavily rely on the IAC models.

In flashing bubbly flows, the interfacial area changes as a function of flow conditions and fluid properties, which usually occurs much more intensely than in conventional boiling flows. The methods to capture the evolution of IAC can be classified into mono-disperse and poly-disperse[12]. The mono-disperse treatment of gas phase refers to a single value of bubble size in each computational cell. Liao et al.[13] simulated the flashing pipe flow with different prescribed bubble diameters. The

results showed that flashing might not be triggered when the bubble diameter is too large. The optimal bubble diameter for flashing onset and development of gas volume fraction was obtained only through case-by-case tuning. Le et al.[14] and Liao and Lucas[15] assumed a constant bubble number density in the simulation of flashing nozzle flow to allow the growth of bubbles. However, discrepancies in the radial distribution of vapor phase were observed due to neglecting bubble coalescence and breakup, which have strong impact on the estimation of bubble number density. In general, the mono-disperse method is limited to situations with constant or narrow distributed bubble size and number density.

For practical flashing flows, a broad spectrum of bubble sizes is always present owing to violent phase change and interactions among phases. A poly-disperse approach is therefore indispensable to trace the interfacial topological information. So far, the poly-dispersity of bubble size or number density in flashing flows has rarely been studied in literature. In general, the poly-disperse methods for bubbly flow can be divided into two categories, one tracking the average parameters of the bubble size distribution such as total number and IAC, while the other tracking the distribution itself. For describing flashing nozzle flows Janet et al.[16] introduced a transport equation for bubble number concentration. Additional closure models for nucleation, coalescence and breakup were included in the source terms. Ooi et al.[17] compared various forms of the interfacial area transport equation (IATE) method (one-group decoupled, one-group coupled, two-group coupled) with flow-regime dependent static correlations for a wide range of flashing flow cases caused by hydrostatic pressure drop. It was found that the two-group IATE is more capable of predicting high void fraction flashing flows than other options. Note that in both Janet et al.[16] and Ooi et al.[17], the size distribution of bubbles (within each group for two-group IATE) is not accounted for. Based on the database ranging from bubbly flow to churn-turbulent flow, Wang et al.[18] derived the source and sink terms of the two-group IATE by assuming a lognormal bubble size distribution for the spherical bubbles and improved the prediction of bubble expansion from the spherical to distorted group, but these progresses have not yet been validated for flashing flows. The poly-dispersity of bubble size can also be achieved by

tracking the distribution directly with a discrete population balance model (PBM). Liao et al.[19] investigated the bubble dynamics in a flashing pipe flow by coupling TFM with the multi-size-group (MUSIG) approach, which is a discrete PBM or class method in ANSYS CFX. The effects of nucleation, phase change, bubble coalescence on the local bubble size distribution is considered through additional closure models while bubble breakup was neglected. According to Liao[20], the MUSIG model in ANSYS CFX is an internally inconsistent method for tackling the breakup process, which violates the bubble number conservation. To overcome this limitation, an alternative discrete scheme for the breakup term in PBM is put forward by Liao et al.[21] and recently implemented in the open-source code OpenFOAM[22]. However, the evaluation of this new method is confined to the validation tests of pure breakage processes, and the extending of its applicability to phase change flow remains to be explored. Li et al.[23] proposed a stability criterion for solving the population balance equation when describing bubble growth and shrinkage in flashing flows.

Even though the TFM-PBM coupled approach provides an important step towards a detailed description of the interfacial structure, more closure models for physical sub-phenomena of flashing flows are required, the choice of which may affect the prediction accuracy of the sophisticated approach. The importance of further research on interfacial heat transfer in flashing flows has also been discussed in Ooi et al.[17]. To validate the reliability of the closures for tackling the simulation of flashing flows, a series of numerical tests based on OpenFOAM code is performed in the present work. To the best of the author's knowledge, the poly-disperse flashing simulation in the frame of TFM with OpenFOAM has not been reported yet. Furthermore, the OpenFOAM PBM model is an improved discrete method in comparison to the MUSIG in CFX, which is crucial for the evaluation of closures.

The remainder of this paper is structured as follows. Section 2 begins with a brief description of the mathematical models. Section 3 carries out preliminary tests of the static bubble growth, which mainly focuses on the phase change term in PBM. Numerical simulations of flashing pipe flows focusing on interfacial heat transfer and bubble coalescence and breakup are presented in Section 4. Conclusions and

suggestions are summarized in Section 5. All the numerical experiments are performed on basis of the multiphaseEulerFoam solver in OpenFOAM-8 with HZDR addons[24].

2. Mathematical model

The numerical study is performed in the framework of coupled TFM-PBM. Considering that the TFM theory and its fundamental transport equations have been described at length in many references, e.g. Drew[25], Ishii and Hibiki[26], Liao et al.[27], the mathematical description is focused on the main closure models that relate to interfacial mass, momentum and heat transfer and the PBM. The latter provides the Sauter mean bubble diameter (or IAC) and considers relevant bubble dynamics phenomena in phase change such as nucleation, growth, coalescence and breakup.

2.1 Main closure models

Interfacial mass transfer during flashing process takes place through three typical forms: nucleation, inertia-controlled phase change, and thermal-controlled phase change[28]. Assuming pressure equilibrium across the interface, the inertial-controlled terms can be neglected. Thus, the interfacial mass transfer is given by:

$$\Gamma_{\mathrm{g}} = -\Gamma_{\mathrm{l}} = \Gamma_{\mathrm{N}} + \Gamma_{\mathrm{T}} \tag{1}$$

where Γ_{g}, Γ_{l} denote the mass transfer from interface to the gas and liquid phase, and Γ_{N}, Γ_{T} represent the part due to nucleation and heat transfer, respectively.

Considering that the superheat in flashing flows is relatively low, the contribution from homogeneous nucleation is ignored[16]. Furthermore, heterogeneous nucleation can be divided into two types, namely, bulk nucleation and wall nucleation. The former is omitted in the present study to avoid uncertainty introduced by the adjustable parameters, such as the heterogeneous factor and the number density of impurities in the bulk fluid. Thus, the mass source term arising from wall nucleation is given by:

$$\Gamma_{\mathrm{N}} = \frac{\pi d_{\mathrm{dep}}^3}{6} \rho_{\mathrm{g}} J_{\mathrm{HET,w}} \frac{S_{\mathrm{f}}}{V_{\mathrm{c}}} \frac{d_1}{d_{\mathrm{dep}}} \tag{2}$$

where d_{dep} is departure diameter of bubbles, S_{f} the wall-sided surface area, V_{c} the volume of the cells adjacent to the wall, and d_1 is bubble diameter of size class 1 in PBM, which will be explained in more detail in the following section. The factor $S_{\mathrm{f}} / V_{\mathrm{c}}$ transforms the surface source to a volumetric one, while the correction term d_1 / d_{dep} is

introduced to ensure the conservation of IAC as the nucleated bubbles are assigned to the size class 1. $J_{\mathrm{HET,w}}$ is wall nucleation rate given by the Shin-Jones model[29]:

$$J_{\mathrm{HET,w}} = f_{\mathrm{dep}} N_{\mathrm{N}} = 2.5\times10^{-4}\left(T_{\mathrm{l}} - T_{\mathrm{sat}}\right)^{3} \frac{r_{\mathrm{dep}}^{2}}{r_{\mathrm{c}}^{4}} \tag{3}$$

where f_{dep} is departure frequency, N_{N} nucleation site density, T_{sat} saturation temperature, and r_{dep} and r_{c} are departure radius and critical radius, respectively.

Bubble growth or shrinkage during thermal-controlled phase change stage is driven by the temperature difference between the gas and liquid phases. The gas phase and gas-liquid interface are assumed to remain at the saturation condition corresponding to the local pressure, then Γ_{T} is expressed as:

$$\Gamma_{\mathrm{T}} = \frac{h_{\mathrm{lg}} A_{\mathrm{i}} \left(T_{\mathrm{i}} - T_{\mathrm{l}}\right)}{H_{\mathrm{il}} - H_{\mathrm{ig}}} \tag{4}$$

where A_{i} is the IAC whose calculation will be discussed in the following section, T_{i} the interface temperature, which is kept as the saturation temperature, and h_{lg} is the heat transfer coefficient (HTC) between the liquid and the interface. A variety of correlations are available in the literature for the estimation of h_{lg}. The Plesset-Zwick correlation [30] which is derived theoretically by considering the heat conduction between vapor bubbles and surrounding liquid is selected for bubble growth cases:

$$Nu = \frac{12}{\pi} Ja \tag{5}$$

The classical Ranz-Marshall correlation [31] and Liao [32] correlation considering both conduction and convection are considered for simulating the flashing pipe flows.

$$Nu = \underbrace{2}_{NuCond} + \underbrace{0.6 Re_{\mathrm{g}}^{1/2} Pr_{\mathrm{l}}^{1/3}}_{NuConv} \tag{6}$$

$$Nu = \underbrace{\frac{12}{\pi} Ja}_{NuCond} + \underbrace{\frac{2}{\sqrt{\pi}} Pe^{1/2}}_{NuConv} + \underbrace{\frac{2}{\sqrt{\pi}} Pe_{\mathrm{turb}}^{1/2} \frac{d_{\mathrm{g}}}{l_{\mathrm{turb}}}}_{NuTurb} \tag{7}$$

where Ja, Re, Pr, Pe, and Pe_{turb} are Jakob number, Reynold number, Prandtl number, Péclet number and turbulent Péclet number, respectively. Pe_{turb} is defined by the turbulence length and velocity scale, l_{turb}, u_{turb}, where $l_{\mathrm{turb}} = C_{\mu}^{3/4} k^{3/2}/\varepsilon$ and $l_{\mathrm{turb}} = C_{\mu}^{1/4} k^{1/2}$, with the value of 0.09 for the constant C_{μ}, k and ε as turbulent kinetic energy and dissipation rate. It is worth stressing that the two correlations account for heat

conduction and convection in slightly different ways, for example, the Liao correlation relating the conduction to the Jakob number while the Ranz-Marshall correlation using an asymptotic value of 2. In addition, the former models the turbulence effect separately and superposes it with heat conduction and convection linearly.

The latent and sensible heat flow rate transferring from gas-liquid interface to phase k (=l for liquid or g for gas) is given by:

$$Q_k = \Gamma_{\mathrm{T}} H_{\mathrm{ik}} + h_{\mathrm{lg}} A_{\mathrm{i}} \left(T_{\mathrm{i}} - T_k \right) \tag{8}$$

It is worth mentioning that in the present work the gas phase is assumed to be always at the saturation condition.

The interfacial forces $\boldsymbol{F}_{\mathrm{k}}$ acting on each phase include drag force, lift force, wall force, and turbulent dispersion force. The turbulence in the liquid phase is obtained by the k-ω SST model, while gas is considered laminar. The bubble-induced turbulence (BIT) is modelled with Ma correlation[33]. All the closures for interfacial forces and turbulence are referred to the baseline model and summarized in Table 1. Due to the limited space, the reader is referred to Liao et al.[34] for more information.

Table 1. Closure models for the momentum equation.

Term		Reference
Interfacial force	Drag force	Ishii and Zuber[35]
	Lift force	Tomiyama et al,[36]
	Wall force	Hosokawa et al.[37]
	Turbulent dispersion force	Burns et al.[38]
	Virtual force	Constant virtual mass coefficient, $C_{\mathrm{vm}} = 0.5$
Turbulence	Liquid	k-ω SST[39]
	BIT	Ma et al.[33]

2.2 Population balance model

The IAC required for the computation of the interfacial mass, momentum and heat transfer is provided by the population balance model considering the poly-dispersity of the bubbles. The PBM implemented in the multiphaseEulerFoam solver is solved by the class method [19]. The dispersed gas phase is partitioned into a number of size classes, the physical sub-phenomena affecting the evolution of bubble size distribution is considered through source and sink terms for each class. The transport equation for size fraction involving nucleation, thermal-controlled phase change, bubble

coalescence and breakup can be written as:

$$\frac{\partial\left(\rho_{\mathrm{g}}\alpha_{\mathrm{g}} f_{\mathrm{g},n}\right)}{\partial t}+\nabla\cdot\left(\rho_{\mathrm{g}}\alpha_{\mathrm{g}} f_{\mathrm{g},n}\boldsymbol{u}_{\mathrm{g}}\right)=S_{\mathrm{N,n}}+S_{\mathrm{T,n}}+S_{\mathrm{CB,n}} \tag{9}$$

where $f_{\mathrm{g},n}$ is the size fraction of size class n, defined as $f_{\mathrm{g,n}}=\alpha_{\mathrm{g},n}/\alpha_{\mathrm{g}}$. S_{N} denotes the contribution from nucleation. As aforementioned, it is considered only in the class 1, i.e.

$$S_{\mathrm{N,n}}=\begin{cases}\Gamma_{\mathrm{N}}, & \mathrm{n=1}\\ 0, & \mathrm{n>1}\end{cases} \tag{10}$$

The term $S_{\mathrm{T,n}}$ represents the fraction change in class n due to bubble growth. It includes bubbles growing from the class n-1 and those moving to class n+1. The drift of bubbles between neighborhood classes is dealt with an upwind schema proposed by Kumar[40]. Its accuracy is ensured by applying the stability criterion discussed in the previous work[22]. In other words, the Courant number defined by the growth rate, time step and class width satisfies certain condition.

$$S_{\mathrm{T},n}=\rho_{\mathrm{g}}\alpha_{\mathrm{g}}x_{\mathrm{g},n}\left(W_{\mathrm{g},n}\frac{G_{\mathrm{g},n-1}N_{\mathrm{g},n-1}}{x_{\mathrm{g},n}-x_{\mathrm{g},n-1}}-P_{\mathrm{g},n}G_{\mathrm{g},n}N_{\mathrm{g},n}+E_{\mathrm{g},n}\frac{G_{\mathrm{g},n+1}N_{\mathrm{g},n+1}}{x_{\mathrm{g},n}-x_{\mathrm{g},n+1}}\right) \tag{11}$$

where x, N, G is the bubble representative volume, number concentration, volume change rate, respectively. The relation between the x, N and size fraction f is given by $N=f\alpha_{\mathrm{g}}/x$, and G can be calculated from Γ_{T} [23]. The terms inside the brackets from left to right consider the contribution from the class n-1, n, and n+1, and W, P, E are coefficients taking the following form:

$$W_{\mathrm{g},n}=\begin{cases}0 & n=0 \text{ or } G_{\mathrm{g},n-1}\le 0\\ 1 & \text{else}\end{cases} \tag{12}$$

$$P_{\mathrm{g},n}=\begin{cases}\left(x_{n+1}-x_n\right)^{-1} & n<n_{\max} \text{ and } G_{\mathrm{g},n}>0\\ \left(x_{n-1}-x_n\right)^{-1} & n>0 \text{ and } G_{\mathrm{g},n}<0\\ \left(-x_n\right)^{-1} & \text{else}\end{cases} \tag{13}$$

$$E_{\mathrm{g},n}=\begin{cases}0 & n=n_{\max} \text{ or } G_{\mathrm{g},n-1}\ge 0\\ 1 & \text{else}\end{cases} \tag{14}$$

where $n_{\max}$ is the upper limit of the size classes. The effects of bubble coalescence and

breakup are integrated into the source term $S_{\mathrm{CB,n}}$:

$$S_{\mathrm{CB,n}} = B_{\mathrm{B},n} + B_{\mathrm{C},n} - D_{\mathrm{B},n} - D_{\mathrm{C},n} \tag{15}$$

where $B_{\mathrm{B},n}$ and $B_{\mathrm{C},n}$ are birth rates of bubbles in size class n due to breakup of larger bubbles and coalescence of smaller bubbles. $D_{\mathrm{B},n}$ and $D_{\mathrm{C},n}$ are death rates of bubbles in size class n due to their breakup into smaller bubbles and coalescence with other bubbles to form a larger one. By assuming binary coalescence and breakup the birth and death rates are expressed as

$$B_{\mathrm{B},n} = \rho_{\mathrm{g}}\alpha_{\mathrm{g}} \sum_{i>n} \frac{x_{\mathrm{g},n}}{x_{\mathrm{g},i}} f_{g,i} \left(g\left(x_{\mathrm{g},i}; x_{\mathrm{g},n}\right) + \sum_{j<i} g\left(x_{\mathrm{g},i}; x_{\mathrm{g},j}\right) Y_{inj} \right) \tag{16}$$

$$B_{C,n} = \left(\rho_{\mathrm{g}}\alpha_{\mathrm{g}}\right)^2 \left(\frac{1}{2} \sum_{j\le n} \sum_{k\le n} Q\left(x_{g,j}; x_{g,k}\right) X_{jkn} \frac{f_{g,j} f_{g,k}}{m_{g,j} m_{g,k}} m_{g,n} \right) \tag{17}$$

$$D_{B,n} = \rho_{\mathrm{g}}\alpha_{\mathrm{g}} \left(f_{g,n} \sum_{j<n} g\left(x_{g,n}; x_{g,j}\right) \right) \tag{18}$$

$$D_{C,n} = \left(\rho_{\mathrm{g}}\alpha_{\mathrm{g}}\right)^2 \left(\sum_{j} Q\left(x_{g,n}; x_{g,j}\right) f_{g,n} f_{g,j} \frac{1}{m_{g,j}} \right) \tag{19}$$

Wherein Q, g, denote the kernel functions estimating the coalescence and breakup rates. X, Y are two mass matrices giving the fraction of mass that goes to the group n during the coalescence or breakup of other bubbles, and m_g represents the mass of a bubble. The reader is referred to Liao et al.[41,42] for further information regarding modelling of bubble coalescence and breakup.

After solving the size fraction equation for each class the Sauter mean diameter of all bubbles is calculated by means of its definition:

$$d_{\mathrm{sm}} = \frac{1}{\sum_{n=0} \left(f_{\mathrm{g},n} / d_{\mathrm{g},n} \right)} \tag{20}$$

where $d_{\mathrm{g},\,n}$ is the representative diameter of size class n. With the spherical shape assumption, the IAC can be obtained by:

$$A_{\mathrm{i}} = \frac{6\alpha_{\mathrm{g}}}{d_{\mathrm{sm}}} \tag{21}$$

It is worth emphasizing that at high void fraction the bubbles may deviate significantly from the spherical shape. This effect can be considered in the OpenFOAM TFM-PBM approach by introducing a secondary property as introduced in Lehnigk et

al.[22]. In addition, some hybrid methods have been proposed for improved modeling of multiple interfacial morphologies and flow regime transition, e.g. the GENTOP concept proposed by Hänsch et al.[43] and the multi-field approach implemented in the code NEPTUNE-CFD[44]. By bearing this in mind, the present work focuses on the aspect of interfacial HTC and bubble coalescence and breakup. Furthermore, in all the investigated cases, the majority of bubbles are smaller than 10 mm. In the TOPFLOW flashing pipe flow, although some very large bubbles appear, they contribute very little to IAC.

3. Preliminary test

Static bubble growth is a classical scenario that is often used to validate the analytical and numerical solution of interfacial mass and heat transfer[26,39,40]. In the present work, four test cases of the static bubble growth are firstly carried out to evaluate the performance of PBM in the simulation of two-phase flow with thermal-controlled phase change. The Plesset-Zwick correlation [30] is used to describe the process of bubble growth controlled by heat conduction. The experimental data are taken from Dergarabedian[47], Board and Duffey[48], and Hooper and Abdelmessih[49]. As shown in Table 2, vapor bubbles with different initial sizes grow in liquid with constant superheat from 4.5 K to 38.8 K.

Table 2. Summary of test cases for static bubble growth.

Case	p_∞ (bar)	ΔT (K)	Ja	Nu	d_{ini} (m)
1	1.01	4.5	13.48	51.52	2.7×10^{-4}
2	0.38	9.3	68.60	262.02	1.7×10^{-3}
3	0.37	17	129.54	494.79	2.8×10^{-3}
4	1.01	38.8	116.27	444.11	7.4×10^{-4}

The initial bubble size of each case is specified according to the first data point obtained in the experiments. It is assumed that the bubble growth is beyond the surface-tension controlled regime, and controlled only by heat transfer. A cube with single-cell resolution is utilized as the computational domain, in which the initial conditions related to the pressure, temperature, and superheat are designated. The buoyancy is excluded by setting the gravity acceleration to zero, so that no relative motion occurs between

the vapor and liquid phases. The thermal-controlled phase change that contributes to the change of IAC is considered, and the Nu is calculated by Eq. (8). The bubble size in all cases is equally divided into 56 size classes based on bubble diameter under the premise that the stability condition of PBM for bubble growth proposed by Li et al.[22] is satisfied, i.e. $\bar{C}_{\mathrm{CFL}} \leqslant 0.01$. Note that the average courant number $\bar{C}_{\mathrm{CFL}}$ here is defined by the growth rate and class width of bubbles. In the simulation, an initial void fraction is prescribed, and all bubbles are initially positioned in the first class. Under the constant superheat condition, they grow uniformly. Since the coalescence and breakup of bubbles is neglected, the simulations mimics single-bubble growth process.

Figure 1 shows the evolution of the bubble diameter with various superheat. The predicted values are represented by black solid lines while the experimental data by black markers. It evidences that the Sauter mean bubble diameter calculated by PBM fits well with the measurements, except for Case 4 with the superheat $\Delta T = 38.8$ K. Under constant superheating conditions, heat-conduction controlled bubble growth is known to obey the 1/2 power law asymptotically (bubble radius increases proportionately to the square root of time), which has been captured by PBM as shown in Fig. 2. In the case of large superheat, both the simulation and experiment exhibit still the same power law, but the slope differs. This is supposed to be caused by the limitation of the Plesset-Zwick heat transfer model (Eq. (8)). As discussed in Liao and Lucas [50], even for this simple case, there is no generally applicable model. Correlations available in the literature are all a polynomial of the Jakob number but with different coefficients and exponents, which leads to the deviation in the predicted growing slope and different optimal performance zones. Although heat transfer is one focus of this study, the model improvement work is not extended here, since the flashing flow cases investigated below are all at low Jakob number, where convection and turbulence effects dominate. Nevertheless, the preliminary test proves two points: 1) the capability of the Plesset-Zwick model in describing heat diffusion and evaporation at low liquid superheat, 2) the capability of PBM in predicting pure bubble growth.

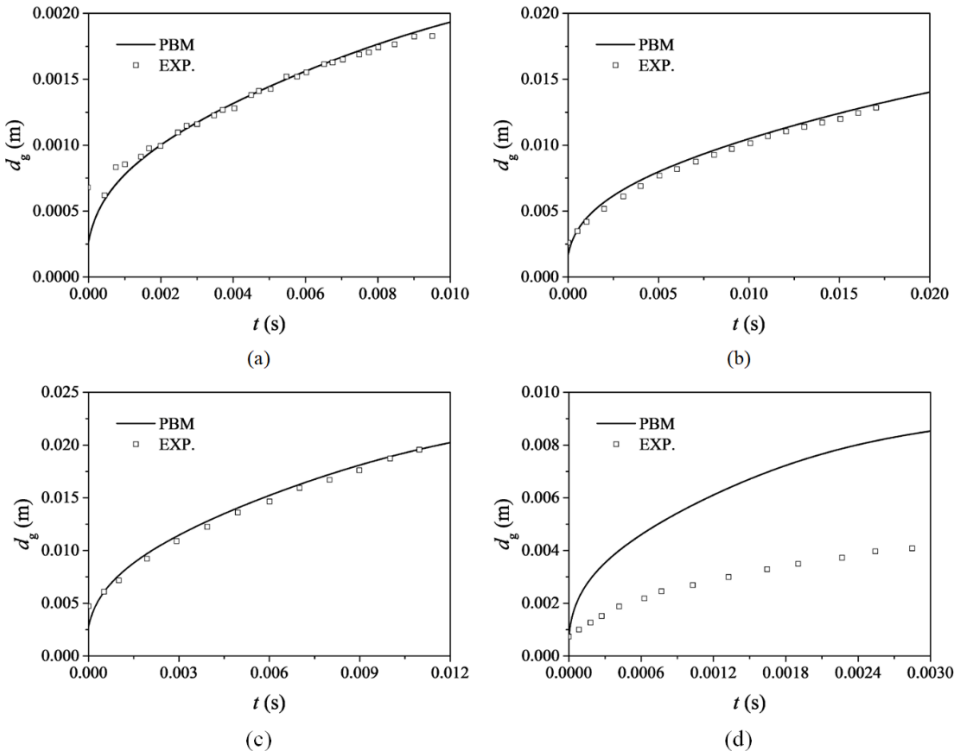

Fig. 1. Numerical and experimental bubble diameter: (a) Case 1: $\Delta T = 4.5\,\mathrm{K}$; (b) Case 2: $\Delta T = 9.3\,\mathrm{K}$; (c) Case 3: $\Delta T = 17\,\mathrm{K}$; (d) Case4: $\Delta T = 38.8\,\mathrm{K}$.

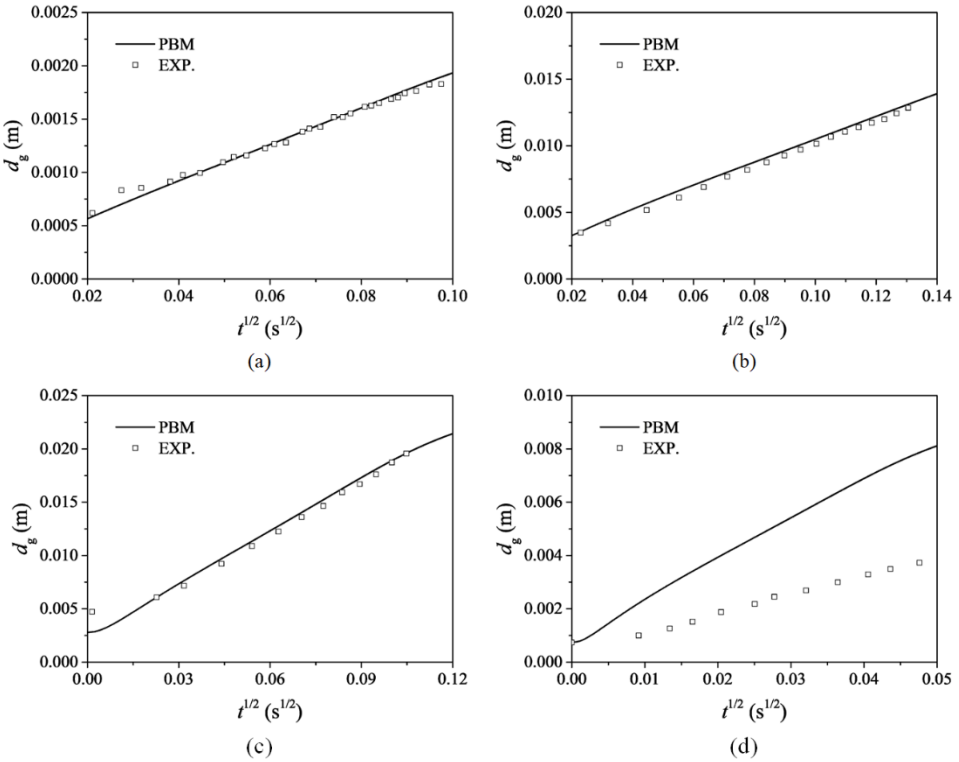

Fig. 2. 1/2 law of bubble growth: (a) Case 1: $\Delta T = 4.5\,\mathrm{K}$; (b) Case 2: $\Delta T = 9.3\,\mathrm{K}$; (c) Case 3: $\Delta T = 17\,\mathrm{K}$; (d) Case4: $\Delta T = 38.8\,\mathrm{K}$.

4. Numerical simulation of flashing pipe flow

4.1 Pressure release experiment

The pressure release experiment of flashing pipe flow is carried out at the TOPFLOW facility of the Helmholtz-Zentrum Dresden-Rossendorf. A detailed information for the facility can be found in Lucas et al.[51]. The main test section consists of an 8 m long vertical pipe with an inner diameter of 195.3 mm. During the experiment, subcooled water flows upwards through the pipe with a velocity around 1 m/s. The depressurization process of the pipe is controlled by a blow-off valve located above the stream drum connected with the outlet of the pipe, where saturation conditions are always guaranteed, but the temperature of the inlet water at the test section is subcooled due to its lower elevation. The spatial and temporal distribution of the vapor-liquid mixture is measured by using two high temperature wire-mesh sensors (WMS) at the top of the pipe. As shown in Table 3, four cases of the pressure release experiments under different pressure level and valve-opening degrees are selected to test the performance of PBM in practical flashing simulations. The whole time of each flashing case lasts for 100 s. The opening level of the valve and its duration are represented by L and t_2, respectively, while the opening and closing speed is controlled by t_1.

Table 3. Summary of test cases for flashing pipe flow.

Case	p_{ini} (bar)	T_{ini} (K)	L (%)	t_1 (s)	t_2 (s)	Ja_{max}
1	10	452.15	50	18	34	0.57
2	10	452.25	60	21	30	0.94
3	20	485.05	40	14	42	0.43
4	20	485.25	50	18	34	0.69

Initially, the water inside the pipe is slightly subcooled, and the temperature is nearly constant owing to low heat loss (<1 kW). During the pressure release transient, the condition in the lower part of the pipe remains below the saturation, while water in the upper part becomes superheated and starts to flash. As the blow-off valve closes again, the flashing is suppressed and the vaporization rate decreases. Finally, the flow inside the pipe returns to single-phase after all steam leaves the domain. A Jakob number indicating the maximum superheat during the process is estimated from the initial temperature and the minimum pressure at the outlet (Table 3). As one can see, the phase change occurs at a quite low Jakob number in all four cases, and the results

of the preliminary tests are applicable. Nevertheless, the phenomena of nucleation, coalescence and breakup lead to a wide range of bubble size. In addition, due to high circulation velocity the effect of turbulence on interfacial heat transfer is significant.

4.2 Simulation setup

To keep the computational cost low, we assume that the flashing flow is axis symmetrical, and 2D simulations are performed. Because the software cannot deal with real 2D geometries, a wedge of 2° is utilized as the computational domain (Fig. 3), and a quasi-2D mesh with one layer of cells in the circumferential direction is applied. Since the wedge angle is sufficiently small, the deviation of the results from real 2D simulations is negligible. The remaining mesh configuration follows the work of Liao and Lucas[19].

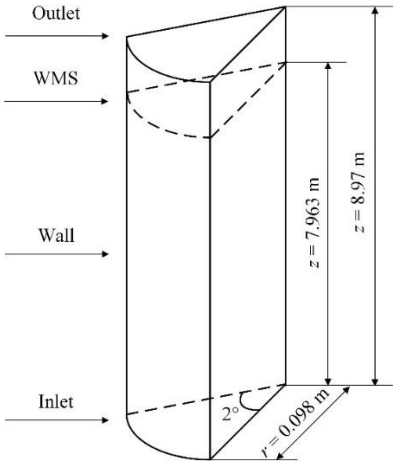

Fig. 3. Schematic of the computational domain (note that the sketch is not to scale).

The transient boundary condition of mass inflow rate, liquid temperature, and outlet pressure are specified based on the experimental data (see Fig. 4). Free-slip and no-slip wall conditions are assigned to the vapor and liquid, respectively, and wedge patch type boundary is used for the front and back of the axis-symmetric geometry. For the turbulent parameters, fully developed single-phase profiles are assumed at the boundaries due to the lack of measurements.

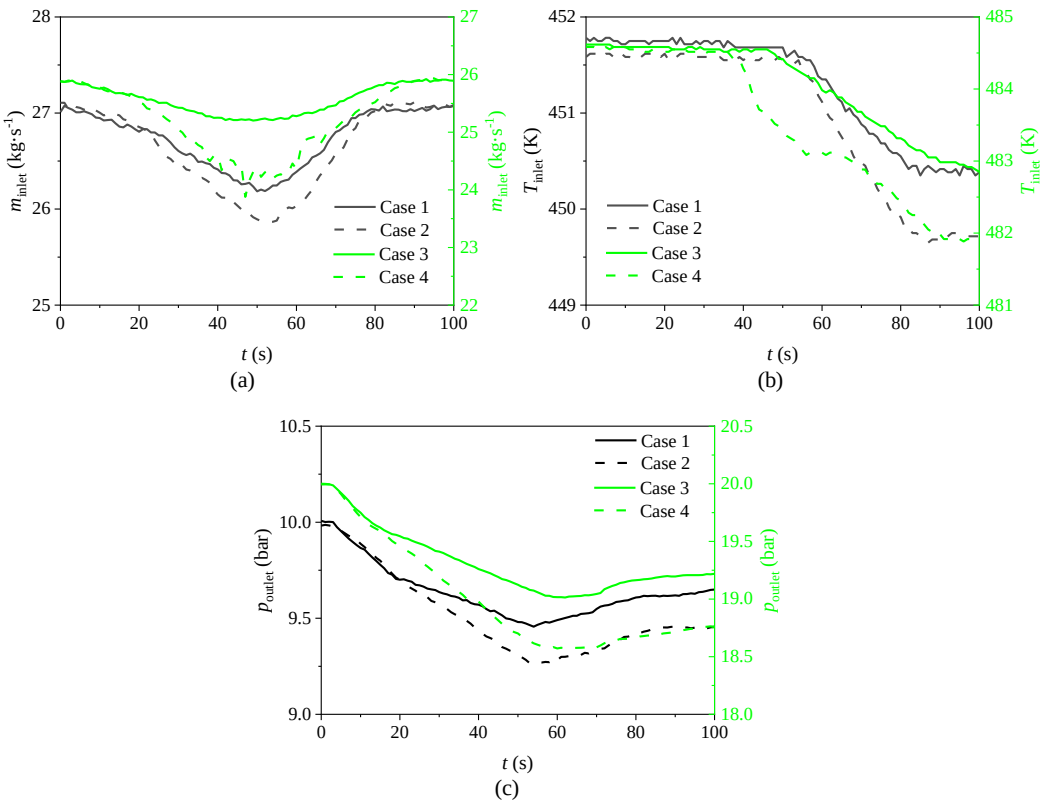

Fig. 4 Boundary conditions provided by experimental data: (a) Inlet liquid mass flow rate; (b) Inlet liquid temperature; (c) Outlet pressure.

The complete mathematical models provided in Section 2 are used to describe the flashing pipe flow, so that important sub-phenomena such as bubble nucleation, growth, coalescence, breakup as well as bubble-induced turbulence are appropriately taken into account. The bubble sizes in PBM are equally divided into 25 size classes with the diameter ranging from 0 to 55 mm. The stability condition regarding bubble growth is determined by the maximum interfacial mass transfer rate, which is calculated from the maximum superheat corresponding to the Ja_{max} of each case. At first, there are no bubbles in all classes. After the flashing is initiated, bubbles generated by nucleation are assigned to the first size class in PBM. Subsequently, they can shift to larger size classes as the result of growth and coalescence, while large bubbles will break up again. The evolution of size distribution is affected by bubble coalescence and breakup as well as interfacial heat transfer. To keep close to the reality, the fluid properties and the saturation conditions are calculated by rewriting the IAPWS-IF97 database[46] into a tabulated form in OpenFOAM and retrieving the values based on the local pressure and

temperature.

The standard interpolation schemes for multiphaseEulerFOAM, which is the TFM solver of OpenFOAM, are used with Gauss linear upwind limited for the velocity component advection term and the stress term. The velocity–pressure coupling is solved using the PIMPLE (merged PISO-SIMPLE) algorithm, thereby, the limit of Courant number less than 1 is overcome and the simulation can be speeded up. The number of outer correction loops is set to 2, which means that the pressure-momentum coupling is calculated twice in one time step.

4.3 Results and discussion

To investigate the effect of interfacial heat transfer and bubble coalescence and breakup, as a first step, a simplified model setup is configured, with only the wall nucleation and thermal-controlled phase change considered in PBM source terms while bubble coalescence and breakup neglected, and the Ranz-Marshall correlation for the evaluation of the HTC. Then, to obtain satisfying distribution of bubble size and gas volume fraction simultaneously, the source and sink terms due to bubble coalescence and breakup is switched on in PBM. Furthermore, turbulence enhancement effect on the interfacial heat transfer is accounted for by using the Liao correlation for *Nu* (Eq. 10). This setup is referred to as improved model configuration. It is however worth mentioning that the Ranz-Marshall correlation is widely used for phase-change dispersed flows. The comparison aims to show the importance of considering bubble coalescence and breakup as well as turbulence enhanced heat transfer in flashing flows.

The prediction of time evolution of gas volume fraction at the WMS with the two model setups is shown in Fig. 5, represented by dashed lines and solid lines, respectively. We first notice that the starting and ending points of flashing corresponding to the valve opening and closing are well captured by PBM. A close look at the profile of the gas volume fraction shows that the maximum gas volume fraction increases with the increase in opening level of the valve under the same initial pressure. This is because the opening level corresponds to the depressurization level. The latter directly controls the superheat and finally affects the interfacial mass transfer rate of the flash evaporation. However, the gas volume fraction calculated by the simplified model

configuration in all cases is apparently lower than the measurements in particular at small valve opening degrees. The under-prediction of gas volume fraction may be related to the neglect of other significant sub-phenomena, such as bubble coalescence and breakup, which affects the evolution of IAC or bubble size distribution. Besides that, the Ranz-Marshall correlation, which is proposed for the evaporation of spherical water drops in hot air stream, is insufficient in calculating the HTC for flashing pipe flows. Detailed comparison of the heat transfer coefficient and heat flux is given below. Though the deviations between numerical and experimental results still exist, the gas volume fraction predicted by the improved approach is closer to the experimental data compared with the simplified one, especially in Case 2 and Case 3. It proves that the turbulence-enhanced convection play a key role in the interfacial transfer.

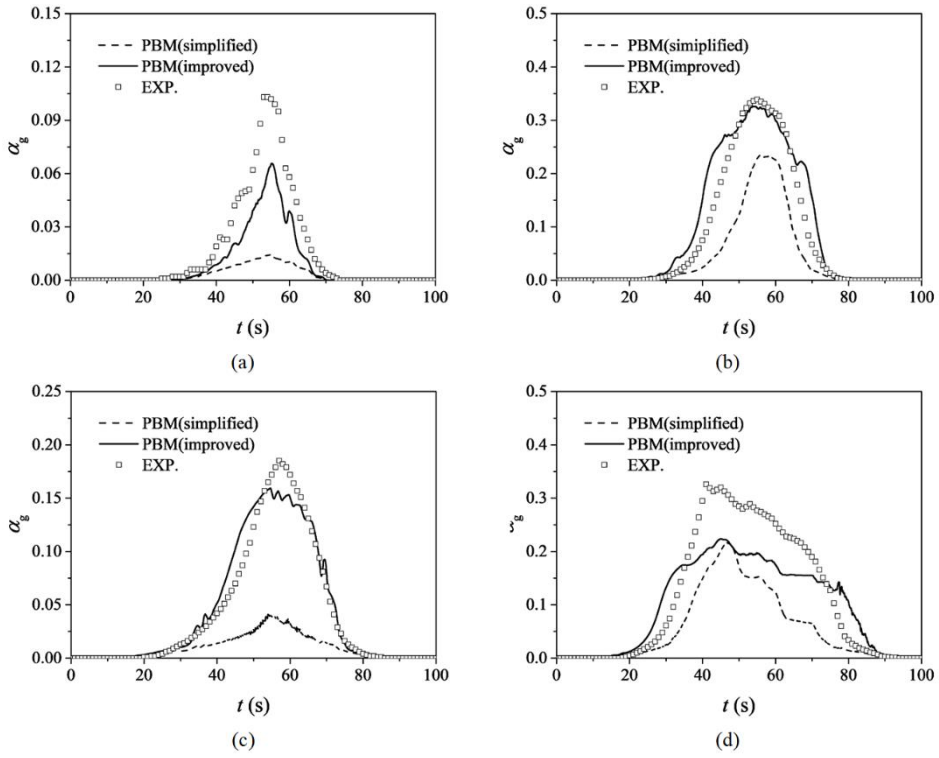

Fig. 5. Improved prediction of evolution of surface averaged gas volume fraction at the WMS: (a) Case1: p_{ini} = 10bar, L = 50%; (b) Case2: p_{ini} = 10bar, L = 60%; (c) Case 3: p_{ini} = 20bar, L = 40%; (d) Case 4: p_{ini} = 20bar, L = 50%.

Defining the bubble size distribution as the gas volume fraction of each size class by the class width, i.e., $\Delta\alpha_g$ / Δd_g, the evolution of bubble size during the pressure release transient is analyzed. The integral over all the bubble size classes is equal to the total gas volume fraction. Taking t = 55 s as an example to verify the bubble size

distribution predicted by PBM, the numerical results against the measurements at the WMS is presented in Fig. 6. Obviously, the bubble diameter is under-predicted by PBM with the simplified model configuration, particularly for the cases with large opening level of the blow-off valve (Case 2 and Case 4). This is because the mechanism that facilitate the increase in bubble size, such as the bubble coalescence, is neglected in the present simulation. Meanwhile, Liao and Lucas [50] reviewed the heat transfer correlations that have been adopted in flashing simulations. They found that the widely accepted Ranz-Marshall correlation is prone to underestimate the heat transfer rate among phases, and thus the bubble growth process is inevitably suppressed. Note that bubble size increases with the heat transfer and evaporation rate, which however in turn suppresses the transfer rate. One can speculate that if the bubble size conforms, the predicted void fraction will be even lower, since the IAC decreases as bubble size increases.

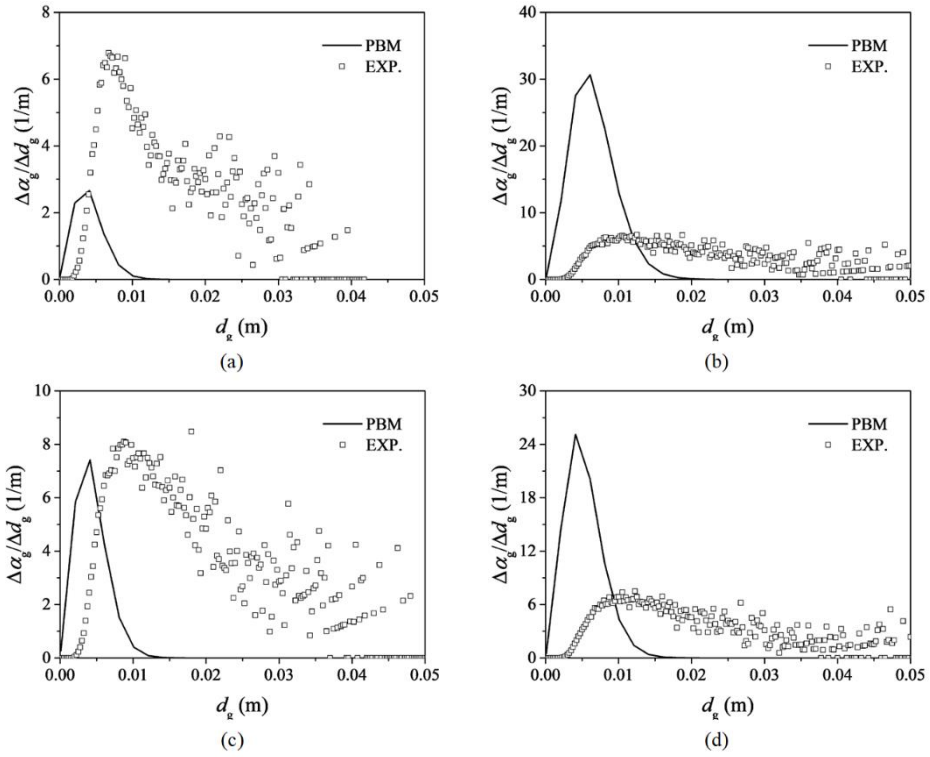

Fig. 6. Bubble size distribution at the WMS at $t = 55$ s: (a) Case1: $p_{ini} = 10$bar, $L = 50\%$; (b) Case2: $p_{ini} = 10$bar, $L = 60\%$; (c) Case 3: $p_{ini} = 20$bar, $L = 40\%$; (d) Case 4: $p_{ini} = 20$bar, $L = 50\%$.

The bubble size distribution with the improved model configuration is given in Fig. 7 for three time points. Compared with the results in Fig. 6, the newly calculated bubble size distribution has been promoted dramatically. In Case 2 and Case 4, the increase of

bubble size is obviously faster than Case 1 and Case 3 because of a larger valve-opening degree (see Table 3). A bimodal distribution is observed in both experiment and simulation. Large bubbles are formed due to coalescence and rapid growth, while simultaneously small bubbles are produced by nucleation and breakup. Note that in Case 2 and Case 4 large plugs or slugs with a diameter over 150 mm are measured, but in the simulation a limit of 55 mm was defined to reduce the computational cost. This leads to the accumulation of bubbles in the last size class of PBM as shown in Fig.7(b) and Fig.7(d), which nevertheless in turn proves the capability of the model in capturing the growth of bubble size. Improved agreement can be achieved by extending the upper limit of bubble size range. Further deviation exists in the peak of small bubbles as well as its position. The peak at t = 29 s can be considered as an indication of nucleation effects, while at other two time points may contain the contribution of bubble breakup. As one can see, in Case 1, the nucleation rate is considerably under-predicted, while in Case 4 over-predicted. The position of the peak is located at a smaller size compared to the measurement. Since the Shin-Jones model was developed for nozzle flow under normal conditions, its applicability to high-pressure conditions needs to be extended. In addition, other nucleation mechanisms like bulk nucleation may play a role considering the high-pressure level. Despite the deviations at the ends, the experiment and simulation match up very well in the major part of the size distribution ($d_g > 0.01$ m), in particular in Case 2 to Case 4. The study shows clearly that the inclusion of bubble coalescence and breakup is important in describing flashing pipe flows with PBM.

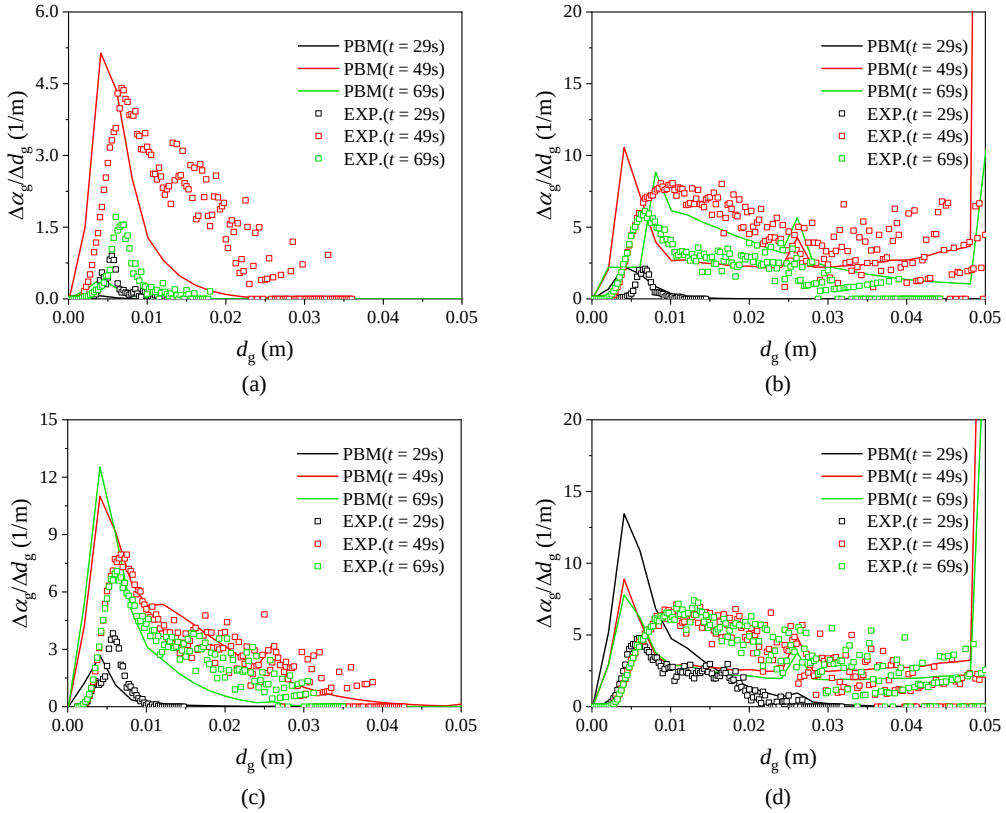

Fig. 7. Improved prediction of bubble size distribution at the WMS: (a) Case 1: p_{ini} = 10bar, L = 50%; (b) Case 2: p_{ini} = 10bar, L = 60%; (c) Case 3: p_{ini} = 20bar, L = 40%; (d) Case 4: p_{ini} = 20bar, L = 50%.

In addition to the averaged quantities, the radial profile of gas volume fraction is also compared in Fig. 8, where r = 0 m and 0.1 m represents the pipe center and wall, respectively. A wall-peak profile indicates the contribution of wall nucleation to bubble generation, and a core-peak profile is a consequence of lateral transport of large bubbles towards the pipe center. With the size increasing from t = 29 s to t = 49 s, bubbles migrate toward the center under the action of lift force. As the void fraction and bubble size decreases during the valve closing stage, bubbles tend to accumulate again in the near-wall region. For Case 4, the core-peaks are apparently observed at t = 49 s and t = 69 s due to the lift force changing its direction for large bubbles. The profile and lateral redistribution are overall captured by the numerical method. Quantitative deviations are mainly attributed to the modelling of IAC and heat transfer discussed above, which has to be polished further, whereas the reliability of interfacial force models for flashing flows and large bubbles has to be revisited as well. Fig.7(c) and Fig.8(c) show that the measured mean size of bubbles exceeds 10 mm at t = 49 s, but their radial distribution

is still wall-peaked, which is inconsistent with the knowledge that in steam-water bubbly pipe flow where the profile changes from wall-peak to core-peak around 4.6 mm with the saturation pressure of 20 bar[53]. The same situation is present in Case 2. In Case 4, the simulation conforms to the experiment, and both give a wall-peak at t = 29 s while a core-peak profile at t = 49 s and t = 69 s. One noticeable point is that a too large Sauter mean diameter, e.g., at t = 49 s in Case 2 and Case 4, tends to lead to a too high accumulation at the pipe center. The effect of bubble size and shape as well as phase change in describing interfacial momentum transfer needs to be considered in the future work.

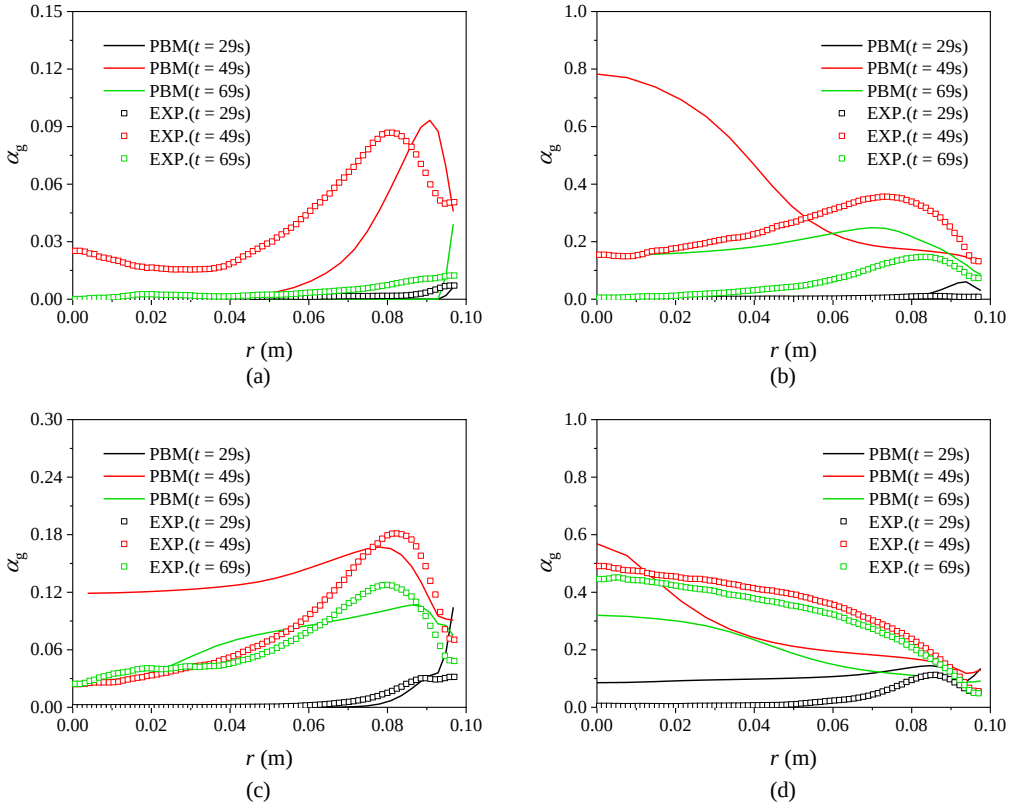

Fig. 8. Radial profile of gas volume fraction at the WMS: (a) Case 1: p_{ini} = 10bar, L = 50%; (b) Case 2: p_{ini} = 10bar, L = 60%; (c) Case 3: p_{ini} = 20bar, L = 40%; (d) Case 4: p_{ini} = 20bar, L = 50%.

The evolution of bubble size and void fraction in flashing flows is directly related to interfacial heat transfer. Higher the heat flux is, larger the bubble size and higher the void fraction. The choice of an appropriate HTC model is the key in the numerical simulation. In this study, two typical models are compared. One is the widely used Ranz-Marshal model and the other is recently proposed by Liao et al. [19, 32]. For the

sake of brevity, the HTC and heat flow rate are extracted from Case 3 to evaluate the interfacial heat transfer behaviors. Similar results are observed in other cases. As shown in Fig. 9(a), the cross-section averaged HTC climbs quickly to a high level before the start of flashing, which is around 20 s (see Fig. 5d). It indicates that flow field is fully developed. During the flashing period (from 20 s to 80 s), the HTC remains almost constant except for some small variations. As discussed before, the HTC predicted by the Ranz-Marshall correlation is smaller than that by the Liao model, and the latter is nearly double of the former. As a result, the sensible heat flux from the superheated liquid to the interface is smaller according to the Ranz-Marshall model, see Fig. 9(b), and the evaporation rate is smaller according to the thermal phase change model (Eq.(4)).

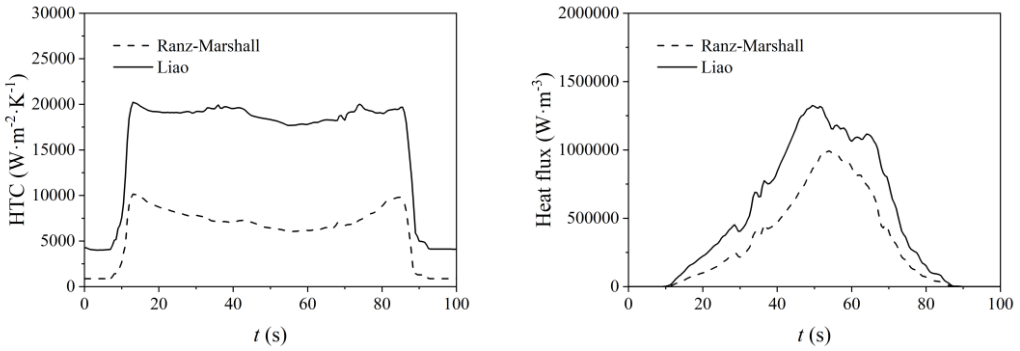

(a) (b)

Fig. 9. Interphase heat transfer coefficient (a) and volumetric heat transfer rate (b) for Case 3: p_{ini} = 20bar, L = 40%, and the influence of HTC model

For further analyzing the heat transfer mechanisms, the Nusselt number (*Nu*) as well as its components is plotted in Fig. 10. According to the Ranz-Marshall model, *Nu* consists of two parts, *NuCond* and *NuConv* (see Eq. (6)). The former represents the heat transfer capacity under the condition of no relative motion, which is referred to as the conduction part in this work. Ranz and Marshall [31] approximate it with an asymptotic value of 2. Figure 10(a) evidences that the convection part *NuConv* contributes majorly to the heat transfer. As presented in Eq. (7), the Liao model accounts for the enhancement effect of turbulence additionally, *NuTurb*, which is comparable to *NuConv* (see Fig.10(b)), and both parts are considerably larger than that of the Ranz-Marshall

model. Furthermore, *NuCond* is proportional to the Jakob number, which is relatively small in the investigated cases (see Table 3), and makes a contribution smaller than 0.8. Note that the dependence of *NuCond* on the Jakob number is the same as the Plesset-Zwick model, which has been validated in the preliminary test for low superheat cases (see section 3).

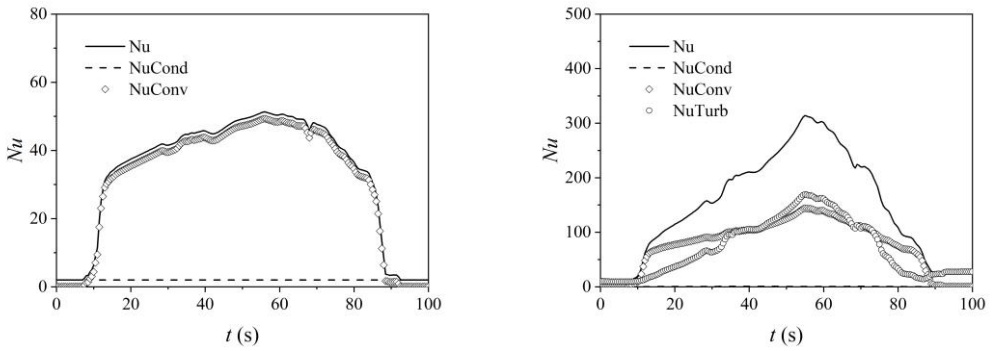

(a) (b)

Fig. 10. Overall Nusselt number and its components of conduction, convection and turbulence calculated by Ranz-Marshall model (a) and Liao model (b) for Case 3: p_{ini} = 20bar, L = 40%

5. Conclusions

Flashing is a kind of phase change phenomena encountered in various industries. Different from the traditional boiling, flashing is induced by depressurization. In the simulation of flashing bubbly flow, the TFM is often utilized as a powerful tool to describe the interfacial transfer process. The interfacial area concentration is a significant parameter that determines the interfacial mass transfer and affects the performance of TFM. The methods calculating the interfacial area concentration can be classified into the mono-disperse and poly-disperse, the latter one is more appropriate for flashing simulation due to the presence of a broad spectrum of bubble size. The present work aims to test the reliability of OpenFOAM PBM model as well as the effect of closures for interfacial heat transfer and bubble coalescence and breakup.

The PBM is first validated for thermal-controlled bubble growth in stagnant superheated liquid. The time evolution of bubble size agrees well with both experimental data and analytical solution. To verify the ability of PBM in practical flashing simulation, where additional source terms are required, four test cases from the

TOPFLOW pressure release experiment series with different pressure levels and depressurization rates are studied. As a simplified model configuration, only the source terms of wall nucleation and phase change are considered. Comparison with measurements reveals that the TFM-PBM approach predicts the onset and cease of flash evaporation during the operation of the blow-off valve successfully, but the gas bubble size and volume fraction is obviously under-predicted. The results show that in turbulent flashing pipe flows, PBM is necessary for predicting the IAC accurately, but bubble coalescence and breakup have to be considered and reliable closures for interfacial heat transfer are required. The following conclusions can be drawn from this paper for the study of interphase heat transfer in flash evaporation processes.

1) In the ideal case without translational motion between the bubbles and the surrounding liquid, the heat transfer is governed by heat diffusion. The capability of existing (semi-)analytical correlations depends on liquid superheat. The well-known Plesset-Zwick model is found to work satisfactorily for low to moderate superheats, while tend to over-predict the heat transfer at high superheats.
2) The situation in practical cases, e.g. turbulent pipe flows, is highly complex, where the convection and effects of slip and turbulence play an important role. The widely used Ranz-Marshall correlation under-predicts the heat transfer coefficient and thus the evaporation rate significantly. By considering the turbulence enhancement through a turbulent Péclet number, the prediction of the averaged gas volume fraction is remarkably promoted.

Besides the flow conditions, recently Li et al.[54] showed that, the deformation and oscillation of bubbles have an effect on the heat transfer by means of DNS studies. In summary, modelling of interfacial heat transfer in practical flashing flows remains a challenge, which needs identify the dominant mechanisms and choose a proper correlation. A general model, which is still missing, should be able to combine all heat transfer mechanisms in a consistent way and take into account the influential factors associated with both fluid flow and interface features.

Acknowledgements

The authors would like to thank the Chinese Scholarship Council (CSC) who supports the present work.

References

[1] D. Moya, C. Aldás, P. Kaparaju, Geothermal energy: Power plant technology and direct heat applications, Renewable and Sustainable Energy Reviews. 94 (2018) 889–901. https://doi.org/10.1016/j.rser.2018.06.047.

[2] T.Y. Lin, C.Y. Ko, S.J. Chen, G.C. Tsai, H.C. Tsai, A novel total-flow geothermal power generator using Turgo turbine: Design and field tests, Renewable Energy. 186 (2022) 562–572. https://doi.org/10.1016/j.renene.2022.01.007.

[3] H. Lv, Y. Wang, L. Wu, Y. Hu, Numerical simulation and optimization of the flash chamber for multi-stage flash seawater desalination, Desalination. 465 (2019) 69–78. https://doi.org/10.1016/j.desal.2019.04.032.

[4] K. Al bkoor Alrawashdeh, K.K. Al-Zboon, L.A. Al-samrraie, R. Momani, T. Momani, E. Gul, P. Bartocci, F. Fantozzi, Performance of dual multistage flashing - recycled brine and solar power plant, in the framework of the water-energy nexus, Energy Nexus. 5 (2022) 100046. https://doi.org/10.1016/j.nexus.2022.100046.

[5] H. Guo, L. Nocivelli, R. Torelli, Numerical study on spray collapse process of ECN spray G injector under flash boiling conditions, Fuel. 290 (2021) 119961. https://doi.org/10.1016/j.fuel.2020.119961.

[6] J. Lu, X. Liu, C. Hu, Z. Li, H. Zheng, S. Li, Experimental study on flashing spray characteristics of pressure swirl nozzle with ethanol solution, Experimental Thermal and Fluid Science. 112 (2020) 110015. https://doi.org/10.1016/j.expthermflusci.2019.110015.

[7] S.K. Rachakonda, Y. Wang, R.O. Grover, M. Moulai, E. Baldwin, G. Zhang, S. Parrish, R. Diwakar, T.W. Kuo, D.P. Schmidt, A computational approach to predict external spray characteristics for flashing and cavitating nozzles, International Journal of Multiphase Flow. 106 (2018) 21–33.

https://doi.org/10.1016/j.ijmultiphaseflow.2018.04.012.

[8] Z.F. Zhou, J. Yin, X.Y. Yang, B. Chen, B. Liu, Experimental investigation on the macroscopic spray and microscopic droplet diameter, velocity and temperature of R404A flashing spray, International Journal of Heat and Mass Transfer. 177 (2021) 121546. https://doi.org/10.1016/j.ijheatmasstransfer.2021.121546.

[9] Z.F. Zhou, G.Y. Lu, B. Chen, Numerical study on the spray and thermal characteristics of R404A flashing spray using OpenFOAM, International Journal of Heat and Mass Transfer. 117 (2018) 1312–1321. https://doi.org/10.1016/j.ijheatmasstransfer.2017.10.095.

[10] H. Yu, Z. Chen, J. Cai, Accident tolerant fuel thermal hydraulic behaviors evaluation during loss of coolant accident in CPR1000, Annals of Nuclear Energy. 139 (2020) 107273. https://doi.org/10.1016/j.anucene.2019.107273.

[11] X. Hou, Z. Sun, G. Fan, L. Wang, Experimental and analytical investigation on the flow characteristics in an open natural circulation system, Applied Thermal Engineering. 124 (2017) 673–687. https://doi.org/10.1016/j.applthermaleng.2017.05.201.

[12] Y. Liao, D. Lucas, Possibilities and Limitations of CFD Simulation for Flashing Flow Scenarios in Nuclear Applications, Energies. 10 (2017) 139. https://doi.org/10.3390/en10010139.

[13] Y. Liao, D. Lucas, E. Krepper, R. Rzehak, Flashing evaporation under different pressure levels, Nuclear Engineering and Design. 265 (2013) 801–813. https://doi.org/10.1016/j.nucengdes.2013.09.027.

[14] Q.D. Le, G. Besagni, F. Inzoli, R. Mereu, Numerical Investigation of Flash Boiling Flow Inside Nozzle: Sensitivity Analysis on Turbulence Modeling Approaches, (2018) 213–230. https://doi.org/10.1615/ichmt.2017.310.

[15] Y. Liao, D. Lucas, 3D CFD simulation of flashing flows in a converging-diverging nozzle, Nuclear Engineering and Design. 292 (2015) 149–163. https://doi.org/10.1016/j.nucengdes.2015.06.015.

[16] J.P. Janet, Y. Liao, D. Lucas, Heterogeneous nucleation in CFD simulation of

flashing flows in converging-diverging nozzles, International Journal of Multiphase Flow. 74 (2015) 106–117. https://doi.org/10.1016/j.ijmultiphaseflow.2015.04.005.

[17] Z.J. Ooi, V. Kumar, C.S. Brooks, Validation of the Interfacial Area Transport Equation Coupled with the Void Transport Equation for Prediction of Flashing Flows, Nuclear Science and Engineering. 194 (2020) 598–619. https://doi.org/10.1080/00295639.2020.1732123.

[18] G. Wang, X. Yang, Q. Zhu, M. Ishii, Evaluation of two-group interfacial area trasport equation in a small pipe and improvement at bubbly to slug transition flow, in: 17th International Topical Meeting on Nuclear Reactor Thermal Hydraulics, NURETH 2017, 2017.

[19] Y. Liao, D. Lucas, Numerical analysis of flashing pipe flow using a population balance approach, International Journal of Heat and Fluid Flow. 77 (2019) 299–313. https://doi.org/10.1016/j.ijheatfluidflow.2019.05.005.

[20] Y. Liao, Update to the MUSIG model in ANSYS CFX for reliable modelling of bubble coalescence and breakup, Applied Mathematical Modelling. 81 (2020) 506–521. https://doi.org/10.1016/j.apm.2020.01.033.

[21] Y. Liao, R. Oertel, S. Kriebitzsch, F. Schlegel, D. Lucas, A discrete population balance equation for binary breakage, International Journal for Numerical Methods in Fluids. 87 (2018) 202–215. https://doi.org/10.1002/fld.4491.

[22] R. Lehnigk, W. Bainbridge, Y. Liao, D. Lucas, T. Niemi, J. Peltola, F. Schlegel, An open-source population balance modeling framework for the simulation of polydisperse multiphase flows, AIChE Journal. 68 (2022). https://doi.org/10.1002/aic.17539.

[23] J. Li, Y. Liao, D. Lucas, P. Zhou, Stability analysis of discrete population balance model for bubble growth and shrinkage, International Journal for Numerical Methods in Fluids. 93 (2021) 3338–3363. https://doi.org/10.1002/fld.5036.

[24] F. Schlegel, K.G. Bilde, M. Draw, I. Evdokimov, S. Hänsch, V.V. Kamble, H. Khan, B. Krull, R. Lehnigk, J. Li, H. Lyu, R. Meller, G. Petelin, M. Tekavčič,

HZDR Multiphase Addon for OpenFOAM, Helmholtz-Zentrum Dresden-Rossendorf. (2022). https://doi.org/10.14278/rodare.1742.

[25] D.A. Drew, Mathematical Modeling of Two-Phase Flow, Annual Review of Fluid Mechanics. 15 (1983) 261–291. https://doi.org/10.1146/annurev.fl.15.010183.001401.

[26] M. Ishii, T. Hibiki, Thermo-Fluid Dynamics of Two-Phase Flow, Springer New York, New York, NY, 2011. https://doi.org/10.1007/978-1-4419-7985-8.

[27] Y. Liao, D. Lucas, E. Krepper, Application of new closure models for bubble coalescence and breakup to steam-water vertical pipe flow, Nuclear Engineering and Design. 279 (2014) 126–136. https://doi.org/10.1016/j.nucengdes.2014.02.015.

[28] G.A. Pinhasi, A. Ullmann, A. Dayan, Modeling of flashing two-phase flow, Reviews in Chemical Engineering. 21 (2005) 133–264. https://doi.org/10.1515/REVCE.2005.21.3-4.133.

[29] T.S. Shin, O.C. Jones, Nucleation and flashing in nozzles-1. A distributed nucleation model, International Journal of Multiphase Flow. 19 (1993) 943–964. https://doi.org/10.1016/0301-9322(93)90071-2.

[30] M.S. Plesset, S.A. Zwick, The growth of vapor bubbles in superheated liquids, Journal of Applied Physics. 25 (1954) 493–500. https://doi.org/10.1063/1.1721668.

[31] W.E. Ranz, R. Marshall, Evaporation from drops 1, Chem. Engng. Prog. 48 (1952) 173–180.

[32] Y. Liao, E. Krepper, D. Lucas, A baseline closure concept for simulating bubbly flow with phase change: A mechanistic model for interphase heat transfer coefficient, Nuclear Engineering and Design. 348 (2019) 1–13. https://doi.org/10.1016/j.nucengdes.2019.04.007.

[33] T. Ma, C. Santarelli, T. Ziegenhein, D. Lucas, J. Fröhlich, Direct numerical simulation–based Reynolds-averaged closure for bubble-induced turbulence, Physical Review Fluids. 2 (2017) 034301. https://doi.org/10.1103/PhysRevFluids.2.034301.

[34] Y. Liao, T. Ma, E. Krepper, D. Lucas, J. Fröhlich, Application of a novel model for bubble-induced turbulence to bubbly flows in containers and vertical pipes, Chemical Engineering Science. 202 (2019) 55–69. https://doi.org/10.1016/j.ces.2019.03.007.

[35] M. Ishii, N. Zuber, Drag coefficient and relative velocity in bubbly, droplet or particulate flows, AIChE Journal. 25 (1979) 843–855. https://doi.org/10.1002/aic.690250513.

[36] A. Tomiyama, H. Tamai, I. Zun, S. Hosokawa, Transverse migration of single bubbles in simple shear flows, Chemical Engineering Science. 57 (2002) 1849–1858. https://doi.org/10.1016/S0009-2509(02)00085-4.

[37] S. Hosokawa, A. Tomiyama, S. Misaki, T. Hamada, Lateral migration of single bubbles due to the presence of wall, American Society of Mechanical Engineers, Fluids Engineering Division (Publication) FED. 257 (2002) 855–860. https://doi.org/10.1115/FEDSM2002-31148.

[38] A.D. Burns, T. Frank, I. Hamill, J.M. Shi, The Favre averaged drag model for turbulent dispersion in Eulerian multi-phase flows, 5th International Conference on Multiphase Flow. (2004) 1–17. http://www.drthfrank.de/publications/2004/Burns_Frank_ICMF_2004_final.pdf.

[39] F.R. Menter, Two-equation eddy-viscosity turbulence models for engineering applications, AIAA Journal. 32 (1994) 1598–1605. https://doi.org/10.2514/3.12149.

[40] J. Kumar, Numerical approximations of population balance equations in particulate systems, 2006. http://diglib.uni-magdeburg.de/Dissertationen/2006/jitkumar.htm.

[41] Y. Liao, R. Rzehak, D. Lucas, E. Krepper, Baseline closure model for dispersed bubbly flow: Bubble coalescence and breakup, Chemical Engineering Science. 122 (2015) 336–349. https://doi.org/10.1016/j.ces.2014.09.042.

[42] Y. Liao, D. Lucas, Poly-disperse simulation of condensing steam-water flow

inside a large vertical pipe, International Journal of Thermal Sciences. 104 (2016) 194–207. https://doi.org/10.1016/j.ijthermalsci.2016.01.016.

[43] S. Hänsch, D. Lucas, E. Krepper, T. Höhne, A multi-field two-fluid concept for transitions between different scales of interfacial structures, International Journal of Multiphase Flow. 47 (2012) 171–182. https://doi.org/10.1016/j.ijmultiphaseflow.2012.07.007.

[44] S. Mimouni, M. Boucker, J. Laviéville, A. Guelfi, D. Bestion, Modelling and computation of cavitation and boiling bubbly flows with the NEPTUNE_CFD code, Nuclear Engineering and Design. 238 (2008) 680–692. https://doi.org/10.1016/j.nucengdes.2007.02.052.

[45] A. Prosperetti, M.S. Plesset, Vapour-bubble growth in a superheated liquid, Journal of Fluid Mechanics. 85 (1978) 349–368. https://doi.org/10.1017/S0022112078000671.

[46] Y. De-wen, X. Zejun, X. Jianjun, Numerical Investigation of Bubble Growth and movement of Subcooled Boiling in Narrow Rectangular Channel, Science and Technology of Nuclear Installations. m (2016).

[47] P. Dergarabedian, The rate of growth of vapor bubbles in superheated water, Journal of Applied Mechanics. 20 (1953) 537–545. https://doi.org/10.1115/1.4010761.

[48] S.J. Board, R.B. Duffey, Spherical vapour bubble growth in superheated liquids, Chemical Engineering Science. 26 (1971) 263–274. https://doi.org/10.1016/0009-2509(71)83001-4.

[49] F.C. Hooper, Abdelmessih，A.H., The flashing of liquids at higher superheats, in: International Heat Transfer Conference 3, Chicago, 1966: pp. 44–50.

[50] Y. Liao, D. Lucas, Evaluation of interfacial heat transfer models for flashing flow with two-fluid CFD, Fluids. 3 (2018). https://doi.org/10.3390/fluids3020038.

[51] D. Lucas, M. Beyer, L. Szalinski, Experiments on evaporating pipe flow, in: The 14th International Topical Meeting on Nuclear Reactor Thermalhydraulics, NURETH-14, Toronto, Ontario, Canada, 2011: pp. 1–13.

[52] W. Wagner, J.R. Cooper, A. Dittmann, J. Kijima, H.-J. Kretzschmar, A. Kruse, R. Mareš, K. Oguchi, H. Sato, I. Stöcker, O. Šifner, Y. Takaishi, I. Tanishita, J. Trübenbach, T. Willkommen, The IAPWS Industrial Formulation 1997 for the Thermodynamic Properties of Water and Steam, Journal of Engineering for Gas Turbines and Power. 122 (2000) 150–184. https://doi.org/10.1115/1.483186.

[53] E. Krepper, D. Lucas, T. Frank, H.M. Prasser, P.J. Zwart, The inhomogeneous MUSIG model for the simulation of polydispersed flows, Nuclear Engineering and Design. 238 (2008) 1690–1702. https://doi.org/10.1016/j.nucengdes.2008.01.004.

[54] J. Li, Y. Liao, I.A. Bolotnov, P. Zhou, D. Lucas, Q. Li, L. Gong, Direct numerical simulation of heat transfer on a deformable vapor bubble rising in superheated liquid, Physics of Fluids. 35 (2023) 023319. https://doi.org/10.1063/5.0137675.